ENERGY OF INTRINSIC MODE FUNCTION FOR GAS-LIQUID FLOW PATTERN IDENTIFICATION

Zhiqiang Sun[1], Hui Gong[1,2]

1) Central South University, School of Energy Science and Engineering, , Changsha 410083, China
  (✉ zqsun@csu.edu.cn, +86 731 8887 9863)
2) Central South University, Hunan Key Laboratory of Energy Conservation in Process Industry, Changsha 410083, China

Abstract

Gas-liquid flows abound in a great variety of industrial processes. Correct recognition of the regimes of a gas-liquid flow is one of the most formidable challenges in multiphase flow measurement. Here we put forward a novel approach to the classification of gas-liquid flow patterns. In this method a flow-pattern map is constructed based on the average energy of intrinsic mode function and the volumetric void fraction of gas-liquid mixture. The intrinsic mode function is extracted from the pressure fluctuation across a bluff body using the empirical mode decomposition technique. Experiments adopting air and water as the working fluids are conducted in the bubble, plug, slug, and annular flow patterns at ambient temperature and atmospheric pressure. Verification tests indicate that the identification rate of the flow-pattern map developed exceeds 90%. This approach is appropriate for the gas-liquid flow pattern identification in practical applications.

Keywords: gas-liquid flow pattern, flow-pattern map, pressure fluctuation, bluff body, signal energy, intrinsic mode function, empirical mode decomposition.

1. Introduction

Gas-liquid flows are found everywhere in natural processes and engineering applications. Examples are the bubbles rising in a glass of cold beer as well as the steam condensation in a steam-water heat exchanger. Flow pattern or flow regime is the visualized description of the behaviour and shape of the phase interfaces in gas-liquid flows. For horizontal adiabatic gas-liquid flows, there are four typical patterns-bubble, plug, slug, and annular [1]. Numerous investigations show that it is hardly possible to achieve accurate measurement and control of parameters in a gas-liquid flow system without a clear understanding of its flow pattern [2]. Identification of gas-liquid flow patterns is primarily based on experimental observations. Among these methods, the flow-pattern map is recognized as one of the most effective means to predict the conditions that result in the transition of flow patterns [3-5]. The validity of the transition lines that are plotted on a flow-pattern map to distinguish each of the flow patterns, however, depends heavily on the coordinate system. Although many coordinate systems are used by various researchers, most maps are only valid for some specific set of conditions or fluids. Hence, development of a set of appropriate coordinate system for flow-pattern maps is in imperative need all the same.

The unsteady wake behind a bluff body is a source full of the flow information [6]. Recent researches reveal that there exist some close couplings between the pressure fluctuation in the cylinder wake and the regime of the gas-liquid flow [7-8]. Different from the single-phase Kármán vortex street over a bluff body, however, the fluctuation of gas-liquid wake involves not only the vortex shedding induced by the continuous phase, but contains the impingement

caused by the disperse phase [9-11]. Consequently, the gas-liquid wake fluctuation includes multiple fluid oscillations of wider frequency band than those of single-phase flows. Through proper acquisition and processing of the wake fluctuation signals, it is possible to discern gas–liquid flow patterns successfully.

The objective of this study is to characterize gas-liquid flows in terms of the energy of the intrinsic mode functions (IMFs) embedded in the pressure fluctuation across a bluff body. The extraction of IMFs is accomplished by the empirical mode decomposition (EMD) technique, which is brought forward recently and is particularly suitable for the exploration of the local oscillatory properties in nonlinear and nonstationary signals [12]. The present method mainly consists of three stages − feature extraction, map construction, and identification test, as given in Fig. 1. In the feature extraction stage, the IMFs present in the original pressure fluctuation across a bluff body are extracted by EMD, and the energy of IMF is selected as the feature to discern the flow patterns. We then establish a flow-pattern map based on the IMF energy and the volumetric void fraction. Finally, we verify the identification rate of the flow-pattern map with "unseen" IMF energies.
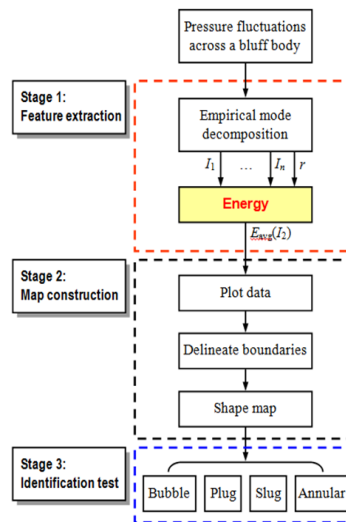

Fig. 1. The process of the proposed method for flow pattern identification.

2. Intrinsic mode function

Intrinsic mode functions are a family of local components embedded in a signal. Each IMF must satisfy two conditions: one is the numbers of extrema and zero crossings either equal or differ at most by one in the whole data set, and the other is the mean value of the envelopes defined by the local maxima and minima is zero at any time. The procedure of extracting IMFs by EMD from signal $x(t)$ is described as follows [8,13].

First of all, identify all the local minima and maxima of $x(t)$, and then use the cubic spline interpolation to define the upper envelope $x_{max}(t)$ and the lower envelope $x_{min}(t)$ of $x(t)$. The mean envelope $m_1(t)$ of the upper and lower envelopes is:

$$m_1(t) = \frac{x_{max}(t) + x_{min}(t)}{2}, \quad (1) \qquad \text{and} \qquad h_1(t) = x(t) - m_1(t). \quad (2)$$

In general, $h_1(t)$ is just an IMF candidate that cannot satisfy all the requirements of an IMF. Iterate the above procedure for k times until the mean envelop is close to zero. So the first IMF $I_1(t)$ that contains the highest frequency component can be designated as:

$$h_{1(k-1)}(t) - m_{1k}(t) = h_{1k}(t), \; I_1(t) = h_{1k}(t). \quad (3)$$

To avoid obliterating the physically meaningful amplitude fluctuations, a stop criterion for the sifting process is predefined by limiting the size of the standard deviation, *SD*, computed from the two consecutive sifting results as:

$$SD = \sum_{t=0}^{T} \left[\frac{\left| h_{1(k-1)}(t) - h_{1k}(t) \right|^2}{h_{1(k-1)}^2(t)} \right]. \tag{4}$$

A typical value for *SD* is set between 0.2 and 0.3.

Separate $I_1(t)$ from the rest of $x(t)$. The residue, $r_1(t)$, is treated as the new data series. Since $r_1(t)$ may still contains much information of lower frequency components, it is subjected to the same sifting process. Repeat the above procedure on the subsequent residual $r_i(t)$ until the residue range is below a predetermined value or the residue contains the lowest frequency component. The result obtained is:

$$r_1(t) - I_2(t) = r_2(t), \cdots, r_{n-1}(t) - I_n(t) = r_n(t), \tag{5}$$

where $r_n(t)$ denotes the trend of the signal, from which no more IMFs can be extracted and I_n is the *n*th IMF.

Each IMF contains lower frequency components than that extracted just before. At the end of EMD, $x(t)$ can be exactly reconstructed using a linear combination:

$$x(t) = \sum_{i=1}^{n} I_i(t) + r_n(t). \tag{6}$$

3. Experiments

Experiments were performed on a gas-liquid two-phase flow test rig with air and water as the working fluids at ambient temperature and atmospheric pressure, as shown in Fig. 2. After the metering of flow rates, the air and water mixed well through a static mixer, then entered into the test section horizontally, and recirculated to the water pool finally. In the test section a bluff body perpendicular to the fluid flow direction, as shown in Fig. 3, was mounted in a circular pipe with an inner diameter $D = 50$ mm.

The cross section of the bluff body was actually a truncated isosceles triangle of width w = 14 mm. Herein the pressure fluctuations across the bluff body were detected by the Duct-wall Differential Pressure Method (DDPM) [14-16] using a dynamic piezoresistive sensor. The two pressure tappings were located 1.0D upstream and 0.2D downstream of the bluff body, respectively. The fluctuating differential pressure signals were acquired by a fast-response digital oscilloscope. The sampling rate of 1 kHz was employed throughout the experiments together with a 10 s holding time. Thus each data set contained 104 points.
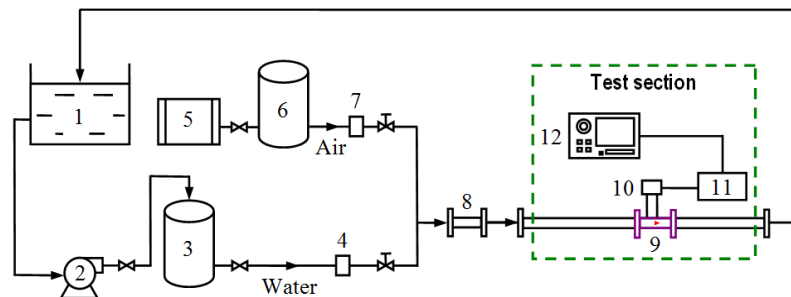

Fig. 2. Schematic of the experimental rig: 1. water pool; 2. pump; 3. water surge tank; 4. Electromagnetic flowmeter; 5. air compressor; 6. air surge tank: 7. gas flowmeter; 8. static mixer; 9. bluff body; 10. differential pressure sensor; 11. signal conditioner; 12. digital oscilloscope.

The upstream and downstream straight pipes connecting the bluff body were $70D$ and $50D$ long, which ensured the flow patterns fully developed in the test section. The flow pattern was recorded manually via a section of transparent pipe installed in front of the bluff body. During the experiments the volumetric flow rates q_{vG} and q_{vL} of air and water were 0.1-130 m^3/h and 0.5–19 m^3/h. The temperature and pressure of the air and water were also measured to obtain their mass flow rates. The total mass flow rate q_{mT} of the gas-liquid mixture was 0.648-18.278 t/h, and the volumetric void fraction β in the test section was 0.017-0.997.
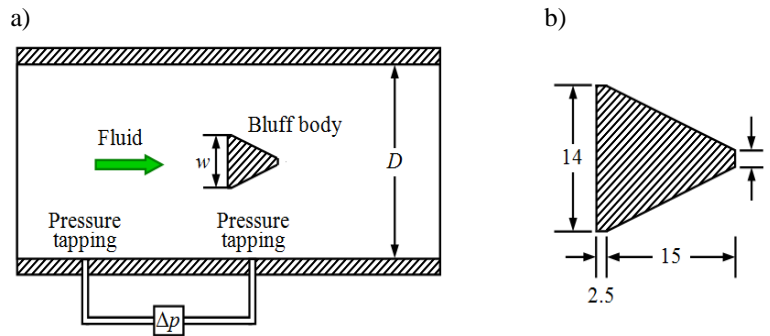

Fig. 3. Longitude-sectional view of the bluff body and the pressure sampling positions:
a) overall structure; b) dimensions of the bluff body (unit: mm).

4. Results and discussion

4.1. Extraction of the energy of intrinsic mode function

The bubble, plug, slug, and annular flow patterns are observed continually under varied fluids conditions in the experiments. Typical raw fluctuating pressure signals across the bluff body and the corresponding IMFs of each flow pattern are illustrated in Fig. 4. The IMF that contains a lower frequency than the preceding one extracted is presented in turn. Each IMF component represents the local characteristics corresponding to the distribution of pressure fluctuation within a certain frequency band. These distributions differ in different IMFs, and undoubtedly contain some inherent properties related to the flow pattern. It is worthwhile to note that the number of the IMFs extracted from the pressure fluctuation signal is actually twelve, according to the points included in each sampled data. Herein only the preceding six IMFs are presented and will be discussed later, because the other components are all of low frequency and weak oscillation. Additionally, the pressure fluctuations and the IMFs obtained under other conditions resemble those in Fig. 4 within the same flow pattern.

Extracting representative features from the acquired signal is paramount to the recognition of the flow pattern. Previous investigations reveal that the energy related characteristics of the pressure fluctuation in gas–liquid flow shift with the variation of flow pattern [17-18]. Hence, such features are suitable to be used as an objective indicator for the monitoring of gas–liquid flow patterns. In this study the average energy of an IMF $I_n(t)$ is defined as:

$$E_{\mathrm{avg}} = \frac{1}{N}\sum_{t=1}^{N} I_n^2(t), \qquad (7)$$

where N is the number of data points in an IMF.

To develop a successful flow-pattern map, minimum number of features need be adopted to reduce the complexity of the construction process. By taking the frequency distribution of IMFs into account, we select the energy of the second IMF I_2 of the pressure fluctuation as the feature to identify the flow patterns.
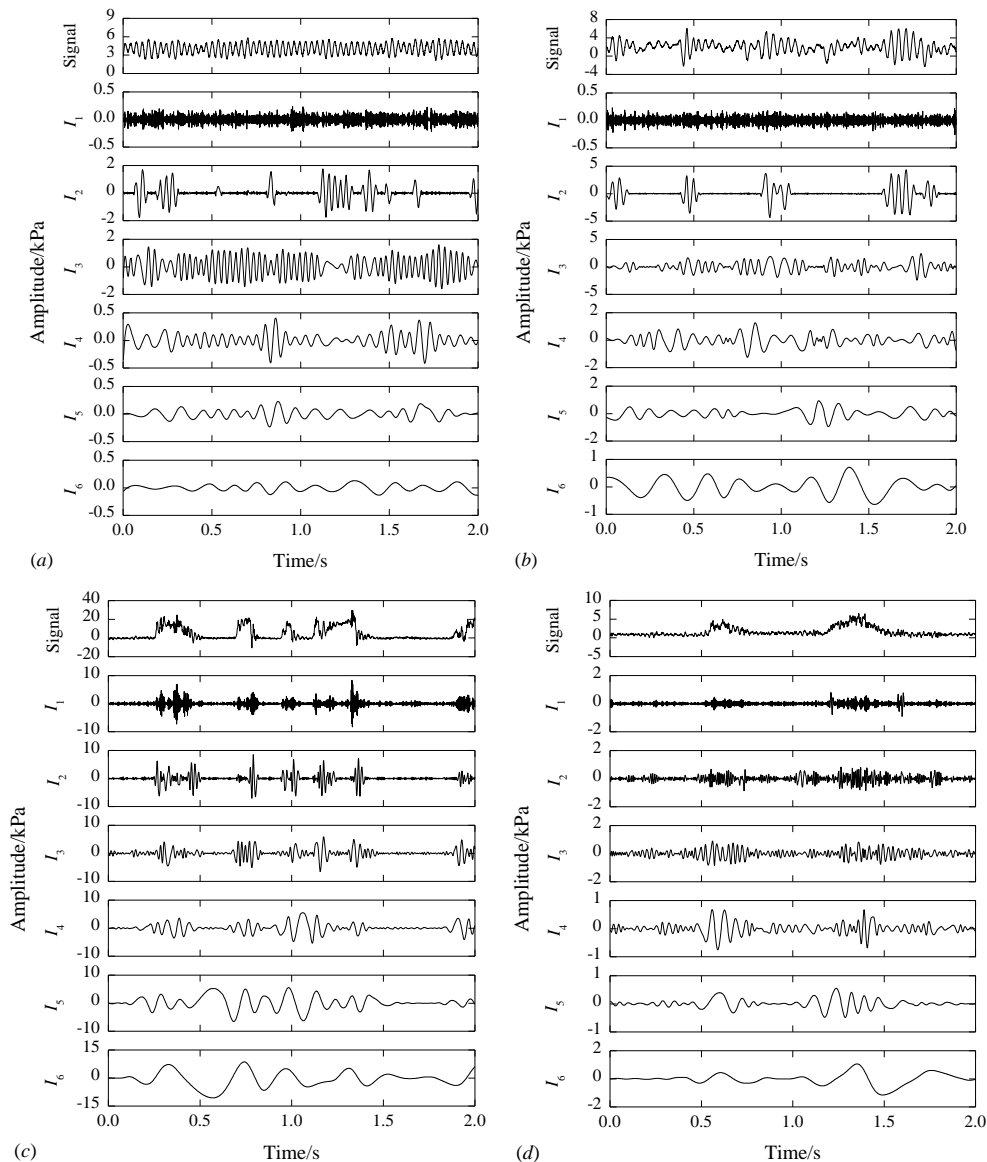
www.czasopisma.pan.pl   PAN   www.journals.pan.pl
POLSKA AKADEMIA NAUK

Metrol. Meas. Syst., Vol. XIX (2012), No. 4, pp. 759-766.

Fig. 4. Partial intrinsic mode functions of the pressure fluctuations in various flow patterns:
a) bubble flow (q_{mT} = 10.95 t/h, β = 0.032); b) plug flow (q_{mT} = 9.31 t/h, β = 0.367);
c) slug flow (q_{mT} = 9.92 t/h, β = 0.657); d) annular flow (q_{mT} = 2.61 t/h, β = 0.978).

4.2. Construction of the flow-pattern map

The foremost task of constructing a flow-pattern map is to define an advisable coordinate system that can distinguish between various flow patterns fairly. The IMF energy represents the intensity of gas-liquid wake fluctuation within a certain band of frequency, so we adopted the average energy E_{avg} of the second IMF I_2 as the vertical coordinate of the flow-pattern map. For the horizontal coordinate, we tentatively employed several flow variables including the total mass flow rate, the volumetric void fraction, the average density, and the two-phase Reynolds number. In the end, we determined to select the volumetric void fraction β as the candidate horizontal coordinate in terms of the distribution of E_{avg} of each flow pattern on the map. The volumetric void fraction β reflects the local structure and trait of phase components, so it is of benefit to the flow pattern identification.

A total of 330 groups of pressure fluctuation data were acquired during the experiments. The number of each flow pattern recorded is listed in Table 1. Following the common practice

of pattern recognition, a fraction of approximately 85% of the total data is selected to construct the flow-pattern maps, which constitutes the construction data. The remainder of the data (test data) is used to verify the flow-pattern map.

Table 1. Numbers of the data for constructing the flow-pattern map and the identification rate.

Flow pattern	Total data	Construction data	Test data	Identified data	Identification rate /%
Bubble	112	95	17	16.5	97.06
Plug	49	42	7	5	71.43
Slug	120	102	18	17.5	97.22
Annular	49	42	7	7	100
Total	330	281	49	46	93.88

As illustrated in Fig. 5, the construction process of the E_{avg}–β flow-pattern map is divided into three steps.
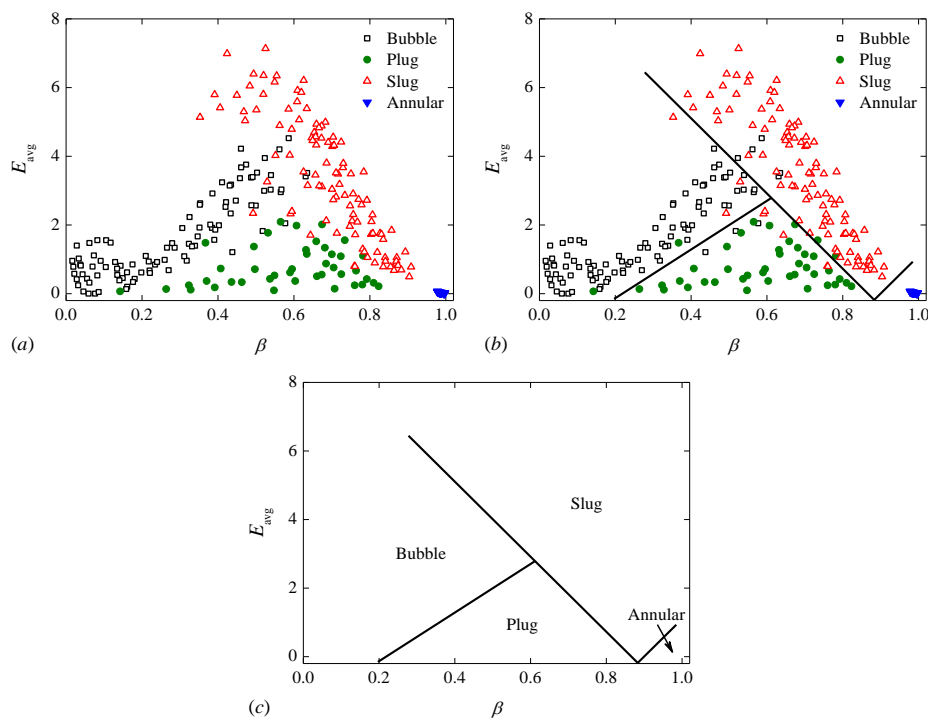

Fig. 5. Construction of the flow-pattern map: a) plot data; b) delineate boundaries; c) shape map.

Step 1: plot data. All construction data are plotted on a plane with the coordinate system of E_{avg} versus β, as shown in Fig. 5a. The distribution of E_{avg} in different flow patterns differs in the range of β, and such differences just provide the rational basis for the discerning of these flow patterns.

Step 2: delineate boundaries. On the coordinated plane with the construction data, the zone of each flow pattern need be established to distinguish it from the others. The general criterion to delineate the boundaries is that we employ mid-separate lines as far as possible to discern each flow pattern region including both the overlapping and the transitional zones, as shown in Fig. 5b.

Step 3: shape map. After the delineation of all the boundaries between flow patterns, the construction data are removed, but the boundaries are reserved. Each region on the plane is then tagged with the name of the flow pattern, and eventually the flow-pattern map takes form as Fig. 5c.

4.3. Test of the flow-pattern map

To examine the effectivity, the test data are plotted on the flow-pattern map constructed, as shown in Fig. 6. If a point of the test data locates wholly on the region of another flow pattern, it is deemed to be a wrong identification. If a test data point happens to fall on the boundaries, it is regarded as half of wrong identification. According to this convention, the identification rate of the E_{avg}–β map is figured out and also listed in Table 1. It is seen that the identification rate of this map is 93.88% in general. Two points of the test data respectively from the bubble and the slug flows lie on the boundary, two points from the plug flow fall in the region of the bubble flow, and the other test data are successfully identified.
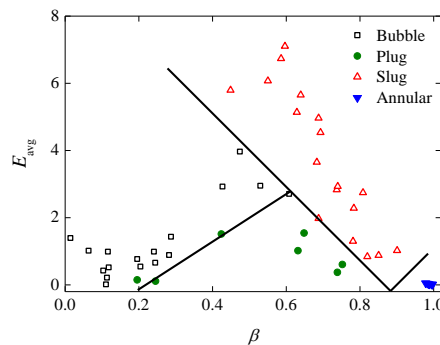

Fig. 6. Test results of the flow-pattern map.

The above results confirm the suitability of adopting the IMF energy as a rational indicator of the gas-liquid flow pattern. Moreover, it reveals that only the neighbouring flow patterns are confused on the proposed map. In view of the nature of the complex interaction between phase interfaces, there assuredly exists concurrence of multiple flow patterns on the boundary of the near-transition conditions.

The gas-liquid flow is a random process strongly affected by phase interactions, pipeline conditions, and environmental factors. The pressure fluctuation induced by the bluff body is therefore time-varying and can be regarded as a strong stochastic time series [19-20]. Since a sample of the fluctuating pressure signal with a finite length is only a snapshot of its ensemble, the features extracted from the sample vary arbitrarily. The identification of gas-liquid flow patterns based on these features is hence fluctuating. The uncertainty in the determination of flow patterns can be lowered by increasing the sample length of the pressure fluctuation with a measuring system of even higher response frequency.

5. Conclusions

In this paper the bubble, plug, slug, and annular flow patterns are identified by a novel flow-pattern map. This map is based on the average energy of intrinsic mode function of the pressure fluctuation across a bluff body and the volumetric void fraction of the gas-liquid mixture. Experiments are conducted on an air-water two-phase flow test rig, and the results show that the overall identification rate of the proposed map exceeds 90%. In view of the absence of any expensive devices and complicated configuration for the same application, this approach is appealing. Another distinctive superiority of the approach is the flow variable that it adopts to constitute the coordinate system of the map. The volumetric void fraction is easy to obtain by conventional instruments. Therefore, this approach provides a cost-effective and practical solution to the gas-liquid flow pattern identification. Nevertheless, subjectivity is unavoidable during the delineation of the boundaries between the observed flow patterns.

More experimental tests are needed to further increase the identification rate and applicability of the flow-pattern map proposed.

Nomenclature: D − inner diameter of pipe; E_{avg} − average energy of intrinsic mode function; I − intrinsic mode function; N − number of data point; n − number of intrinsic mode function; q_{mT} − total mass flow rate of gas–liquid flow; q_{vG} − volumetric flow rate of gas phase; q_{vL} − volumetric flow rate of liquid phase; r − residue; SD − standard deviation; w − width of bluff body; β − volumetric void fraction.

References

[1] Rouhani, S.Z., Sohal, M.S. (1983). Two-phase flow patterns: a review of research results. *Prog. Nucl. Energy*, 11(3), 219-259.

[2] Ramskill, N. P., Wang, M. (2011). Boolean logic analysis for flow regime recognition of gas-liquid horizontal flow. *Meas. Sci. Technol.*, 22(10), 104016.

[3] Baker, O. (1954). Simultaneous flow of oil and gas. *Oil Gas J.*, 53(2), 185-195.

[4] Cheng, L., Ribatski, G., Thome, J.R. (2008). Two-phase flow patterns and flow-pattern maps: fundamentals and applications. *Appl. Mech. Rev.*, 61(1), 050802.

[5] Mandhane, J.M., Gregory, G.A., Aziz, K. (1974). A flow pattern map for gas–liquid flow in horizontal pipes. *Int. J. Multiphas. Flow*, 1(4), 537-553.

[6] Williamson, C.H.K. (1996). Vortex dynamics in the cylinder wake. *An.. Rev. Fluid. Mech.*, 28(1), 477-539.

[7] Sun, Z., Zhang, H. (2008). Neural networks approach for prediction of gas-liquid two-phase flow pattern based on frequency domain analysis of vortex flowmeter signals. *Meas. Sci. Technol.*, 19(1), 015401.

[8] Sun, Z., Zhang, H. (2009). Application of empirical mode decomposition based energy ratio to vortex flowmeter state diagnosis. *J. Cent. South Univ. T.*, 16(1), 154-159.

[9] Hulin, J.P., Fierfort, C., Condol, R. (1982). Experimental study of vortex emission behind bluff obstacles in a gas liquid vertical two phase flow. *Int. J. Multiphas. Flow*, 8(5), 475-490.

[10] Inoue, A., Kozawa, Y., Yokosawa, M., Aoki, S. (1986). Studies on two phase cross flow part I: characteristics around a cylinder. *Int. J. Multiphas. Flow*, 12(2), 149-167.

[11] Shakouchi, T., Tian, D., Ida, T. (2002). Behavior of vertical upward gas−liquid two-phase flow past obstacle in rectangular channel. *JSME Int. J. Ser B-Fluids Therm. Eng.*, 45(3), 686-693.

[12] Huang, N. E., Shen, Z., Long, S. R., Wu, M. C., Shih, H. H., Zheng, Q., Yen, N.C., Tung, C.C., Liu, H.H. (1998). The empirical mode decomposition and the Hilbert spectrum for nonlinear and non-stationary time series analysis. *P. Roy. Soc. A-Math. Phy.*, 454(1971), 903-995.

[13] Sun, Z., Zhou, J., Zhou, P. (2006). Application of Hilbert-Huang transform to denoising in vortex flowmeter. *J. Cent. South Univ. T.*, 13(5), 501-505.

[14] Zhang, H., Huang, Y., Sun, Z. (2006). A study of mass flow rate measurement based on the vortex shedding principle. *Flow Meas. Instru.*, 17(1), 29-38.

[15] Sun, Z., Zhang, H., Zhou, J. (2007). Investigation of the pressure probe properties as the sensor in the vortex flowmeter. *Sensor. Actuat. A-Phys.*, 136(2), 646-655.

[16] Sun, Z., Zhang, H., Zhou, J. (2008). Evaluation of uncertainty in a vortex flowmeter measurement. *Measurement*, 41(4), 349-356.

[17] Sun, B., Zhang, H., Cheng, L., Zhao, Y. (2006). Flow regime identification of gas-liquid two-phase flow based on HHT. *Chinese J. Chem. Eng.*, 14(1), 24-30.

[18] Ding, H., Huang, Z. Y., Song, Z. H., Yan, Y. (2007). Hilbert-Huang transform based signal analysis for the characterization of gas-liquid two-phase flow. *Flow Meas. Instru.*, 18(1), 37-46.

[19] Sun, Z. (2010). Mass flow measurement of gas-liquid bubble flow with the combined use of a Venturi tube and a vortex flowmeter. *Meas. Sci. Technol.*, 21(5), 055403.

[20] Sun, Z., Zhang, H. (2010). Measurement of the flow rate and volume void fraction of gas–liquid bubble flow using a vortex flow meter. *Chem. Eng. Commun.*, 197(2), 145-57.